In Situ Deformations in the Immature Brain During Rapid Rotations

Nicole G. Ibrahim

Rahul Natesh

Spencer E. Szczesny

Karen Ryall

Stephanie A. Eucker

Brittany Coats

Susan S. Margulies
e-mail: margulie@seas.upenn.edu

Department of Bioengineering,
University of Pennsylvania,
240 Skirkanich Hall,
210 South 33rd Street,
Philadelphia, PA 19104-6321

Head trauma is the leading cause of death and debilitating injury in children. Computational models are important tools used to understand head injury mechanisms but they must be validated with experimental data. In this communication we present in situ measurements of brain deformation during rapid, nonimpact head rotation in juvenile pigs of different ages. These data will be used to validate computational models identifying age-dependent thresholds of axonal injury. Fresh 5 days ($n=3$) and 4 weeks ($n=2$) old piglet heads were transected horizontally and secured in a container. The cut surface of each brain was marked and covered with a transparent, lubricated plate that allowed the brain to move freely in the plane of rotation. For each brain, a rapid (20–28 ms) 65 deg rotation was applied sequentially at 50 rad/s, 75 rad/s, and 75 rad/s. Each rotation was digitally captured at 2500 frames/s (480×320 pixels) and mark locations were tracked and used to compute strain using an in-house program in MATLAB. Peak values of principal strain (E_{peak}) were significantly larger during deceleration than during acceleration of the head rotation ($p<0.05$), and doubled with a 50% increase in velocity. E_{peak} was also significantly higher during the second 75 rad/s rotation than during the first 75 rad/s rotation ($p<0.0001$), suggesting structural alteration at 75 rad/s and the possibility that similar changes may have occurred at 50 rad/s. Analyzing only lower velocity (50 rad/s) rotations, E_{peak} significantly increased with age (16.5% versus 12.4%, $p<0.003$), which was likely due to the larger brain mass and smaller viscoelastic modulus of the 4 weeks old pig brain compared with those of the 5 days old. Strain measurement error for the overall methodology was estimated to be 1%. Brain tissue strain during rapid, nonimpact head rotation in the juvenile pig varies significantly with age. The empirical data presented will be used to validate computational model predictions of brain motion under similar loading conditions and to assist in the development of age-specific thresholds for axonal injury. Future studies will examine the brain-skull displacement and will be used to validate brain-skull interactions in computational models. [DOI: 10.1115/1.4000956]

Keywords: brain tissue strains, finite element model validation, brain deformation, pediatric head injury

1 Introduction

Head injury is the most common cause of death or hospitalization among children in the United States [1], affecting more than 16,000 children under age 5 each year. Observed injury types include subdural hematoma and diffuse axonal injury (DAI). Biomechanical analyses of primate and porcine inertial models of DAI indicate a link between brain material response, i.e., tissue strain, and white matter injury [2,3]. This finding is further supported by in vitro evidence that uniaxial tensile strain is closely associated with primary dysfunction in unmyelinated [4] and myelinated [5] axons.

Physical and computational models of the head are used to relate loading conditions (e.g., acceleration, impact force) to brain deformation. Physical models, often made of a mixture of artificial materials and bony tissues [3,6], have been used to estimate brain tissue displacement during rapid movements. The biofidelity of these models depends on how accurately the synthetic materials represent brain material properties (modulus, homogeneity, anisotropy, and viscoelasticity) and how accurately material-bone attachments reproduce the brain-skull interface. Likewise, parametric simulations reveal the dependence of predicted brain deformation on the material properties and boundary conditions assigned to computational models. Despite these findings, model predictions of brain deformation are rarely validated against experimental data.

The majority of empirical brain deformation data in current literature are limited to adults. Early investigations implanting a translucent plastic calvarium on adult Macaque and rhesus monkeys monitored brain motion in vivo using high-speed photography [7,8]. These studies were restricted to cortical surface measurements and could not investigate deeper brain deformations more related to axonal injury. Other studies incorporated flash X-ray cinematography to track relative movements between brain and skull in anesthetized dogs and rhesus monkeys and in intact human cadavers [9–11]. The most recent investigations utilized intravascular contrast media or implanted radio-opaque materials [11–13] to measure relative brain-skull displacement during inertial loading. These studies used only a few widely spaced tracers that may limit their spatial resolution.

No studies to date have measured brain deformations in the rapidly developing immature brain, in which the contributions of smaller size and stiffer material properties [14] may influence brain tissue response to applied loads. The objective of this study was to develop and implement a method to measure intracranial tissue deformations during rapid rotational loading in 5 days and 4 weeks old piglets, whose brain maturational development approximates that of human infants and toddlers, respectively [15,16]. We hypothesized that brain tissue strain would increase with increasing applied angular velocity, and that for the same applied load, strains would be higher in the 4 weeks old than in the 5 days old piglet brain due to its larger mass and lower viscoelastic modulus [14]. The strain data from this study will be used to validate finite element model predictions of porcine brain responses to inertial loading, thus aiding the development of age-specific brain deformation thresholds for axonal injury.

2 Methods

2.1 Model Construction. Physical models were constructed using 5 days ($n=3$) and 4 weeks ($n=2$) old female piglets. Each animal was sacrificed with 150 mg/kg sodium pentobarbital overdose, approved by the University of Pennsylvania IACUC. The

Contributed by the Bioengineering Division of ASME for publication in the JOURNAL OF BIOMECHANICAL ENGINEERING. Manuscript received September 21, 2009; final manuscript received October 8, 2009; accepted manuscript posted January 6, 2010; published online March 10, 2010. Editor: Michael Sacks.

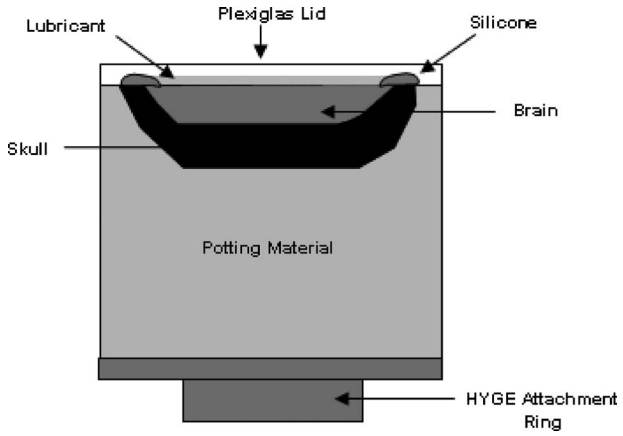

Fig. 1 Diagram of the horizontal transection set-up. The transected brain and skull are potted in the canister with the exposed brain facing out and visible through the transparent lid.

head was separated from the cervical spine and the exterior soft tissues and mandible were removed from the outer skull. The intact skull and cranial contents were transected in a horizontal plane just superior to the orbits and lateral ventricles, using a Dremmel blade to cut the skull and a long knife for the brain and meninges. The depth of the cut plane relative to the skull apex was recorded.

The inferior portion of the transected head was embedded inside a custom-machined cylindrical aluminum canister (Fig. 1) using polymethylmethacrylate (PMMA, Dentsply, York, PA) in a ratio of 1.5 g of powder per milliliter of liquid. The transected head was positioned in the canister with the cut surface facing out and approximately 1 cm from the surface of the PMMA. The inner surface of the canister was lined with petroleum jelly prior to embedding to enable sample removal at the end of the study, and three set screws were inserted through the sides of the canister into the PMMA to prevent movement of the cured resin during the study. There were 35–40 India ink (Speedball Art, Statesville, NC) marks, ~2–3 mm in diameter, placed on the cut brain surface to visualize tissue motion. An additional six to eight marks were placed on the potting material to extract rigid body motion and to assess measurement error. The ink was allowed to dry for 40 min. Saline was applied to the brain surface to prevent the tissue from drying out.

A layer of silicone caulk was applied to the exposed portion of the skull to provide an airtight seal between the skull and Plexiglas cover plate (Fig. 1). The ~1 mm space between the brain surface and cover plate was filled with clear lubricant (KY Brand, Skillman, NJ) to ensure a frictionless boundary condition. The cover plate was secured with screws. All physical models were constructed and used within 5 h of sacrifice.

2.2 Rapid Rotations. The canister was mounted onto one side arm of a previously described linkage that converts linear motion from a pneumatic-driven piston (HYGE, Bendix Corp., Southfield, MI) to a 65 deg rotation [17]. A counterweight was placed on the opposite side arm to provide stability. Each transected head was rotated three times in the anatomic axial plane about a center corresponding to the location of the C2–C4 spinal segment of the animal. The first rotation (run 1) lasted 28 ms with a peak angular velocity of 50 rad/s, the second rotation (run 2) lasted 20 ms with peak angular velocity 75 rad/s, and the final rotation (run 3) repeated the previous load with duration 20 ms and peak angular velocity 75 rad/s. The angular velocity was measured with an angular rate sensor (Model ARS-06, ATA Inc., Albuquerque, NM) attached to the linkage sidearm and the data was acquired at 10 kHz using a PC-based data acquisition system

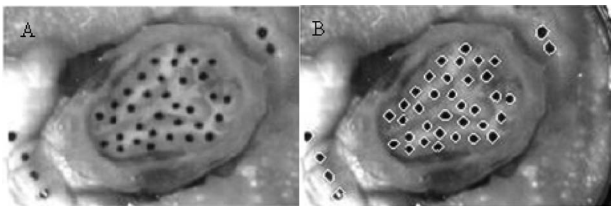

Fig. 2 (*a*) Original cropped frame excluding extraneous background and (*b*) perimeters of identified objects superimposed on cropped image shown in (*a*)

(LABVIEW, National Instruments, Austin, TX). A high-speed (2500 fps) digital camera (HG TH, Redlake, Tallahassee, FL) with a resolution of 480×320 (0.54 mm/pixel) recorded the motion of the container, brain, and ink marks using MOTIONCENTRAL software (Redlake, Tallahassee, FL).

2.3 Image Processing. To remove extraneous background signal, a cropping window was defined based on the first frame and applied to all subsequent frames (Fig. 2(*a*)). The gray-scale images were then filtered to remove artifacts from nonuniform lighting and improve visualization of the ink marks. Using an in-house segmentation program written in MATLAB (The Mathworks Inc., Natick, MA), the brain and potting resin marks in each frame were isolated from the background and labeled as objects in a binary image. The perimeter and centroid of each object in each frame were calculated. The perimeters of all isolated objects were superimposed on the original cropped image for each frame (Fig. 2(*b*)) to verify accurate segmentation of the marks.

The origin of the coordinate system was defined on the potted resin, and coordinates of every object's centroid were tracked in all frames. Objects were excluded from analysis if in any frame they met any of the following criteria: (a) the object was less than 2 pixels in diameter (indistinguishable from noise), (b) the object was too close in proximity to another object and merged during segmentation, or the (c) object became distorted and improperly segmented.

2.4 Data Analysis. Nonoverlapping triads were defined from sets of three closely spaced brain tissue marks. The displacement of the triad centroid was calculated for every triad in every frame, and strain tensors were computed at each centroid. The 2D Lagrangian strain tensors were defined as

$$E_{aa} = \frac{\partial u}{\partial a} + \frac{1}{2}\left[\left(\frac{\partial u}{\partial a}\right)^2 + \left(\frac{\partial v}{\partial a}\right)^2 + \left(\frac{\partial w}{\partial a}\right)^2\right] \tag{1}$$

and

$$E_{ab} = \frac{1}{2}\left[\frac{\partial u}{\partial b} + \frac{\partial v}{\partial a} + \left(\frac{\partial u}{\partial a}\frac{\partial u}{\partial b}\right) + \left(\frac{\partial v}{\partial a}\frac{\partial v}{\partial b}\right) + \left(\frac{\partial w}{\partial a}\frac{\partial w}{\partial b}\right)\right] \tag{2}$$

where u, v, and w are functions of a and b, x, and y coordinates of the triad centroid, respectively. The maximum principal strain ($E_{\max}$) was calculated for each triad in each frame as

$$E_{\max} = \frac{E_{aa} + E_{bb}}{2} + \sqrt{\left(\frac{E_{aa} - E_{bb}}{2}\right)^2 + E_{ab}^2} \tag{3}$$

For each triad, the peak maximum principal strain (E_{peak}) over the entire rotation and the frame number (i.e., time) in which it occurred were recorded. All values were reported as mean ± standard deviation.

3 Results

3.1 Error. Potting resin and brain tissue marks were both used to determine the contribution of error from image processing on strain calculations. Because the potting resin was considered to be a rigid body, triads on the resin would be expected to have

Table 1 Strain values for brain triads during acceleration and deceleration

Animal	Age	Angular velocity (rad/s)	Angular acceleration (krad/s^2)	Angular deceleration (krad/s^2)	Run No.	Avg. accel. E_{max} (%)	Avg. decel. E_{max} (%)
080808	5 days	52	6.2	6.9	1	9.70	10.98
080808	5 days	75	11.1	12.3	2[a]	16.68	23.11
080808	5 days	73	11.9	12.9	3[a]	19.06	27.70
080813	5 days	53	6.7	6.3	1	8.81	11.11
080813	5 days	74	10.5	14.9	2[a]	15.56	25.86
080813	5 days	72	10.0	12.5	3[a]	19.17	33.03
080814	5 days	54	5.5	6.6	1[a]	10.55	14.43
080814	5 days	74	10.9	12.8	2[a]	19.91	30.64
080814	5 days	74	10.1	12.8	3[a]	19.41	32.33
080812	4 weeks	52	7.0	7.1	1[a]	13.25	15.81
080812	4 weeks	76	13.0	13.2	2[a]	20.66	33.54
080812	4 weeks	74	11.4	12.8	3[a]	22.58	39.20
080815	4 weeks	54	5.9	6.6	1[a]	14.87	17.63
080815	4 weeks	73	10.9	13.1	2[a]	21.68	31.26
080815	4 weeks	72	10.3	12.5	3[a]	30.68	37.82

[a]Indicates runs in which maximum principal strains were significantly larger in the deceleration phase compared with acceleration phase.

strains of zero throughout the motion with deviations from zero representing error. To calculate this error, potting resin marks were evaluated for two velocities in two different animals ($n=4$). Calculated resin strains (E_{peak}) averaged $1.02 \pm 0.40\%$, indicating a small but statistically significant ($p=0.014$) measurement error. In a separate error analysis, E_{peak} was calculated for brain triads during 30–60 frames of video filmed before rotational motion commenced using three runs from two different animals ($n=6$). The average strain experienced by brain triads during the stationary frames was $0.98 \pm 0.22\%$, similarly indicating a small but significant ($p<0.001$) measurement error. From these two analyses, we conclude our strain measurement error is approximately 1%.

3.2 Acceleration Versus Deceleration Strains. Peak angular velocities for each head rotation are provided in Table 1. On average there were 28 ± 9 nonoverlapping brain tissue triads visible throughout an entire rotation. During each rotation, the canister experienced an acceleration phase, reaching a peak rotational velocity followed by a deceleration phase. Using a paired student's *t*-test (5% type I error) and analyzing each run separately for each animal, peak maximum principal strains (E_{peak}) during the deceleration phase were significantly ($p<0.05$) larger than those in the acceleration phase for 13 of the 15 runs. In the remaining two runs (both at low velocity), strains were larger during deceleration than acceleration but did not reach significance. Therefore, the remaining analysis was performed comparing deceleration E_{peak} strains only.

3.3 Effect of Rotational Load Magnitude. To determine the effect of increased rotational velocity on tissue strains, E_{peak} for each triad in the lower load (50 rad/s, run 1) was compared with its corresponding E_{peak} during the first higher load (75 rad/s, run 2) in the same animal using a paired student's *t*-test (5% type I error). For both piglet ages, strains approximately doubled with a 50% increase in rotational velocity. The higher velocity produced $26.9 \pm 1.5\%$ strains in 5 days old pigs (62 triads) and $30.5 \pm 1.4\%$ strains in 4 weeks old pigs (48 triads), which were significantly greater than the lower velocity strains in each age group, $12.4 \pm 0.6\%$ and $16.5 \pm 0.7\%$, respectively, ($p<0.0001$).

3.4 Reproducibility. To assess the reproducibility of tissue strain measurements, E_{peak} of the two repeated higher load rotations (runs 2 and 3) were compared at each centroid using a paired student's *t*-test (5% type I error). A total of 48 triads from 5 days old animals and 53 triads from 4 weeks old animals were analyzed. Although load magnitudes were the same, significantly larger strains were observed during the second high velocity run in both ages ($28.7 \pm 1.5\%$ (run 3) versus $25.1 \pm 1.3\%$ (run 2) for 5 days old, $p<0.0001$; $37.5 \pm 1.6\%$ (run 3) versus $32.7 \pm 1.4\%$ (run 2) for 4 weeks old, $p<0.0001$). The small but significant increases in strain observed with the subsequent identical load suggest structural damage to the tissue and/or disruption of the brain-skull interface following the first load. Because it cannot be determined whether such structural changes also occurred following the lower velocity loads (run 1, 50 rad/s), subsequent analysis was limited to data from the low velocity rotations (run 1).

3.5 Effect of Age. To determine whether older animals with larger, softer brains [14] experienced larger strains when subjected to the same rotational load, E_{peak} of the lower loads (run 1) were combined for all 5 days old animals (63 triads) and compared with those of 4 weeks old animals (48 triads). The strains were significantly larger in the older animals compared with the younger animals ($16.5 \pm 0.7\%$ versus $12.4 \pm 0.6\%$, $p<0.003$).

4 Discussion

We have developed and implemented a method to measure brain deformations during rapid rotations in 5 days and 4 weeks old piglet heads, which can be used to validate finite element model predictions of brain response to mechanical loading. We observed an age-related increase in strain response from 5 days old to 4 weeks old brain under similar loading conditions, consistent with the lower elastic modulus of 4 weeks old piglet brain tissue (215.6 Pa) compared with that of 5 days old (526.9 Pa) [14] and the larger brain mass in 4 weeks old (57 g) compared with the 5 days old (37 g) piglets. However, additional age-specific injury strain threshold data are needed to determine whether the larger tissue strains in older animals would result in more severe injuries than the smaller strains in younger animals.

Despite statistically significant strain measurement errors attributable to nonuniform lighting and minor difficulties with edge detection and centroid finding, these errors (1%) were significantly smaller than strains calculated during even the low velocity runs (12–15%). We conclude that measurement error was minimal compared with calculated peak tissue strains.

The brain tissue strain data from these experiments are a crucial first step in validating finite element models of brain deformation. However, several limitations exist in the present study. First, brain strain measurements were two-dimensional and restricted to within the plane of rotation. Strains orthogonal to the rotational plane could not be measured in this study but can be assumed to be minimal compared with strains within the plane of rotation. Second, it is possible that the brain-skull interface was slightly altered during the transection. All precautions were taken while cutting these tissues to maintain the structural integrity of the

brain-skull interface. Last, we found significant differences in strain between the two higher load (75 rad/s) rotations, indicating that some structural changes may have occurred. It is unknown whether similar structural changes occurred following the initial lower velocity rotation (50 rad/s), therefore we limited our brain tissue strain comparisons across age to only this lower velocity run.

Using isolated in vitro optic nerve and axonal stretch preparations, investigators report that axonal elongations of 5–34% are capable of producing structural or functional axonal damage [18–20]. In our in situ preparation we measured 12–15% strain. However, the lower rotational loads used in this study are similar to velocities measured in infant and toddler dummies during head-first occipital impacts from one foot falls or less [21–23], which clinically rarely result in abnormal neurological outcomes in children. We suspect that because the white matter microstructure is undulated [24], an initial strain is required to "straighten" the axons in intact brain tissue prior to axonal elongation. Thus, we would expect in situ brain tissue strains, as measured in our study, to be larger than the strains experienced by the individual axons.

In conclusion, we have developed a head transection model for directly measuring brain tissue strains in situ in a cadaveric preparation. These measurements will aid in understanding age-related brain deformations from rapid head rotations and will be useful in validating computational models of pediatric traumatic brain injury.

Acknowledgment

The authors would like to thank Jill Ralston for her technical expertise throughout the study. Support provided by NIH Grant No. R01NS039679.

References

[1] 2006, "CDC National Vital Statistics Report," Deaths: Injuries, 2001.
[2] Miller, R., Margulies, S., Leoni, M., Nonaka, M., Chen, X., Smith, D., and Meaney, D., 1998, "Finite Element Modeling Approaches for Predicting Injury in an Experimental Model of Severe Diffuse Axonal Injury," Proceedings of the 42nd Stapp Car Crash Conference, SAE, Tempe, AZ, pp. 155–167.
[3] Margulies, S., Thibault, L., and Gennarelli, T., 1990, "Physical Model Simulations of Brain Injury in the Primate," J. Biomech., **23**, pp. 823–836.
[4] Galbraith, J. A., Thibault, L. E., and Matteson, D. R., 1993, "Mechanical and Electrical Responses of the Squid Giant Axon to Simple Elongation," ASME J. Biomech. Eng., **115**, pp. 13–22.
[5] Lusardi, T. A., Smith, D. H., Wolf, J. A., and Meaney, D. F., 2003, "The Separate Roles of Calcium and Mechanical Forces in Mediating Cell Death in Mechanically Injured Neurons," Biorheology, **40**, pp. 401–409.
[6] Ljung, C., 1975, "A Model for Brain Deformation Due to Rotation of the Skull," J. Biomech., **8**, pp. 263–274.
[7] Pudenz, R. H., and Shelden, C. H., 1946, "The Lucite Calvarium—A Method for Direct Observation of the Brain. II. Cranial Trauma and Brain Movement," J. Neurosurg., **3**, pp. 87–505.
[8] Gosch, H. H., Gooding, E., and Schneider, R. C., 1969, "Distortion and Displacement of the Brain in Experimental Head Injuries," Surg. Forum, **20**, pp. 425–426.
[9] Shatsky, S. A., 1973 "Flash X-Ray Cinematography During Impact Injury," Proceedings of the 17tth Stapp Car Crash Conference, pp. 361–376.
[10] Hodgson, V. R., Gurdjian, E. S., and Thomas, L. M., 1966, "Experimental Skull Deformation and Brain Displacement Demonstrated by Flash X-Ray Technique," J. Neurosurg., **25**, pp. 549–552.
[11] Gurdjian, E., Hodgson, V. R., Thomas, L., and Patrick, L., 1968, "Significance of Relative Movement of Scalp, Skull, and Intracranial Contents During Impact Injury of the Head," J. Neurosurg., **29**, pp. 70–72.
[12] Hardy, W. N., Foster, C. D., King, A. I., and Tashman, S., 1997, "Investigation of Brain Injury Kinematics: Introduction of a New Technique," Crashworthiness, Occupant Protection and Biomechanics in Transportation Systems, **225**, pp. 241–254.
[13] Nusholtz, G. S., Lux, P., Kaiker, P. S., and Janicki, M. A., 1984 "Head Impact Response—Skull Deformation and Angular Accelerations," Proceedings of the 28th Stapp Car Crash Conference, pp. 41–74.
[14] Prange, M. T., and Margulies, S. S., 2002, "Regional, Directional, and Age-Dependent Properties of the Brain Undergoing Large Deformation," ASME J. Biomech. Eng., **124**, pp. 244–252.
[15] Duhaime, A. C., 2006, "Large Animal Models of Traumatic Injury to the Immature Brain," Dev. Neurosci., **28**, pp. 380–387.
[16] Missios, S., Harris, B. T., Simoni, M. K., Dodge, C. P., Costine, B. A., Quebada, P. B., Hillier, S. C., Adams, L. B., Duhaime, A. C., and Lee, Y. L., 2009, "Scaled Cortical Impact in Immature Swine: Effect of Age and Gender on Lesion Volume," J. Neurotrauma, **26**(11), pp. 1943–1951.
[17] Raghupathi, R., and Margulies, S. S., 2002, "Traumatic Axonal Injury Following Closed Head Injury in the Neonatal Pig," J. Neurotrauma, **19**, pp. 843–853.
[18] Bain, A. C., Raghupathi, R., and Meaney, D. F., 2001, "Dynamic Stretch Correlates to Both Morphological Abnormalities and Electrophysiological Impairment in a Model of Traumatic Axonal Injury," J. Neurotrauma, **18**, pp. 499–511.
[19] Margulies, S. S., and Thibault, L. E., 1992, "A Proposed Tolerance Criterion for Diffuse Axonal Injury in Man," J. Biomech., **25**, pp. 917–923.
[20] Prange, M. T., 2002, "Biomechanics of Traumatic Brain Injury in the Infant," Bioengineering, University of Pennsylvania, Philadelphia.
[21] Coats, B., and Margulies, S. S., 2008, "Potential for Head Injuries in Infants from Low-Height Falls," J. Neurosurg. Pediatrics, **2**, pp. 321–330.
[22] Ibrahim, N. G., 2009, "Head Injury Biomechanics in Toddlers: Integrated Clinical, Anthropomorphic Dummy, Animal and Finite Element Model Studies," Department of Bioengineering, University of Pennsylvania, Philadelphia, PA.
[23] Ibrahim, N. G., and Margulies, S. S., (1992), "Biomechanics of the Toddler Head During Low Height Falls: An Anthropomorphic Dummy Analysis," J. Neurosurg. Pediatrics (unpublished).
[24] Bain, A. C., Shreiber, D. I., and Meaney, D. F., 2003, "Modeling of Microstructural Kinematics During Simple Elongation of Central Nervous System Tissue," ASME J. Biomech. Eng., **125**, pp. 798–804.